Structural characterization and biological fluid interaction of Sol-Gel derived Mg-substituted biphasic calcium phosphate ceramics.

S. Gomes [a,b], G. Renaudin [a], E. Jallot [b] and J.-M. Nedelec [a*]

[a] Laboratoire des Matériaux Inorganiques CNRS UMR 6002, Université Blaise Pascal & Ecole Nationale Supérieure de Chimie de Clermont-Ferrand, Clermont Université, 24 avenue des Landais, 63177 Aubière Cedex, France.

[b] Laboratoire de Physique Corpusculaire de Clermont-Ferrand CNRS / IN2P3 UMR 6533, Université Blaise Pascal, Clermont Université, 24 avenue des Landais, 63177 Aubière Cedex, France.

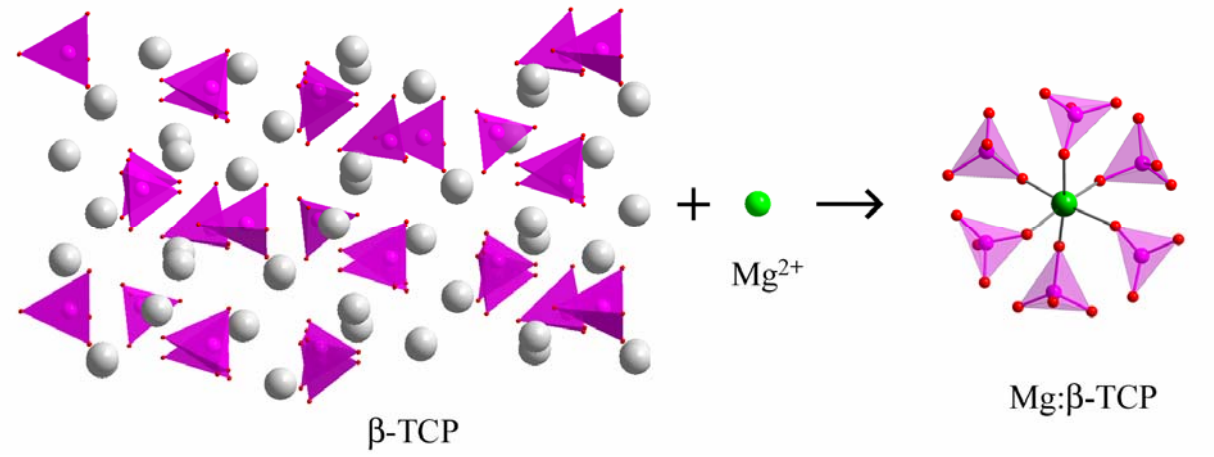

* Corresponding author
J.M. Nedelec Tel 00 33 4 73 40 7195 Fax 00 33 4 73 40 53 28
e-mail : j-marie.nedelec@univ-bpclermont.fr

Abstract

Sol-Gel chemistry has been used to prepare undoped and Mg-substituted biphasic calcium phosphates (BCP) ceramic composed of hydroxyapatite (HAp) and whitlockite (β-TCP) phases. Different series of samples have been synthesized with different Mg doping level (from 0 to 5 atomic % of calcium atoms substituted) and different temperature of calcinations (from 500 to 1100°C). All the powdered samples were systematically treated by Rietveld refinement to extract the quantitative phase analysis, the structural and microstructural parameters, to locate the Mg crystallographic sites and to refine the composition of the Mg-substituted phases. The temperature dependence of the weight amount ratio between HAp and β-TCP is not monotonic due to the formation of minor phases as $Ca_2P_2O_7$, CaO, MgO, $CaCO_3$ and certainly an amorphous phase. On the other hand the Mg stabilizing feature on the whitlockite phase has been evidenced and explained. The mechanism of stabilization by small Mg^{2+} is different to this by big Sr^{2+}. Nevertheless, in both cases, the whitlockite stabilisation is realised by an improvement of the environment of the Ca4 site unusually face coordinated to a PO_4 tetrahedron. The substitution of Mg atom in the Ca5 site allows to improve considerably the bond valence sum of the unusual Ca4 polyhedron. The temperature of calcinations combined with the amount of introduced Mg atoms allow to monitor the phases composition of the BCP ceramic as well as their microstructural properties. The bioactivity properties of the BCP samples are improved by the presence of Mg atoms in the structure of the β-TCP phase. The mechanism of improvement is mainly attributed to an accelerated kinetic of precipitation of a calcium phosphate layer at the surface comprising HAp and/or β-TCP phases.

Keywords: biomaterials, bio-interfaces, biomineralization, calcium phosphates

1. Introduction

Biphasic calcium phosphates (BCP) ceramics, composed of a mixture of hydroxyapatite (HAp, $Ca_5(PO_4)_3OH$) and beta-tri calcium phosphate (β-TCP, β-$Ca_3(PO_4)_2$), are interesting candidates in reconstructive surgery. Bone mineral mass is dominated by nano-crystalline non-stoichiometric HAp [1-3]. For these reasons, HAp has been widely used as biocompatible materials for permanent bone replacement, scaffold for new bone growth or for bone prostheses coating [4]. β-TCP has also been largely considered due to its high solubility in particular in conjunction with HAp to produce so called Biphasic Calcium phosphate (BCP). Advantages of the BCP ceramics are the difference in dissolution properties of the two phases, the rapid bone reconstruction around the implant site and their close matches with the inorganic components of bones [5-7]. The addition of magnesium (the fourth highest concentrated cation in the human body after calcium, potassium and sodium) in BCP is attracting due to the beneficial effects on the physicochemical properties of minerals [8-10] and on the bone metabolism [2,11,12]. Bone minerals contain various amounts of magnesium [13], either adsorbed at the surface of hydroxyapatite crystals or incorporated inside its crystallographic structure [12]. The mineral encountered in biological systems commonly named with the term 'whitlockite' (in the biological and medical literature) is in fact a magnesium substituted whitlockite phase [2,14-17]. The deficiency of Mg in bone has been suggested as a possible risk factor for osteoporosis in humans [11]. Magnesium is known to reduce the degradation rate of calcium phosphate biomaterials [18-20] and to influence the crystallization of mineral substance [12,13,21-27]. The substituted low magnesium-containing apatite sample decreased the osteoinductive properties of biomaterials whereas the substituted high magnesium-containing apatite had a toxic effect on bone cells [12]. In recent years, the development of Mg-substituted hydroxyapatite and/or BCP ceramics has been subject of interest [10,28-30]. The amount of HAp and β-TCP in BCP can be tailored by the temperature of calcination [31,32] as well as by the insertion of magnesium [2,10,21,33,34] or strontium [35,36]. The dissolution properties of both phases can be modified by incorporation of doping elements [37]. The substitution of magnesium during the preparation process of BCP ceramics can also been useful to monitor the microstructural parameters (namely the average crystallite size) of the HAp and β-TCP [10,13,21-27]. The purpose of our study was to examine in detail the incorporation of Mg^{2+} ions in BCP samples at the atomic level: identification and quantification of the crystallised phases, identification of the Mg-occupied crystallographic sites, determination of the chemical composition of the different phases and

determination of the microstrucral parameters (average crystallite size and internal constraints). Rietveld analyses were performed on X-ray diffraction powder patterns recorded from series of BCP samples containing different amount of magnesium (from 0 to 5 atomic % of calcium substituted by Mg) and with different temperature of calcination (from 500 to 1100°C).

2. Experimental

2.1 Sol-Gel elaboration of Mg-substituted BCP

The sol-gel route previously proposed by the authors [38,39] has been used. Briefly, to produce 2 g of pure HAp powder, 4.7 g of $Ca(NO_3)_2{\cdot}4H_2O$ (Aldrich, USA – purity: 99%), 0.84 g of P_2O_5 (Avocado Research chemicals. Ltd, UK - purity: 99%) were dissolved in ethanol under stirring and refluxed at 85°C during 24 h to favour nucleation. Then, this solution was kept at 55°C during 24 h, to obtain a white consistent gel and further dried at 80°C during 10 h to obtain a white powder. Finally, the powder was heated at 1100°C during 15 h (the obtained sample was named 00Mg1100). To prepare Mg-substituted hydroxyapatite, the required amount of $Mg(NO_3)_2.6H_2O$ (Aldrich, USA – purity: 99.999%) was added to the solution. Four Mg-substituted samples were prepared with the Mg substitution levels of 0.5, 1, 2 and 5 atomic % (at. %) of calcium substituted by magnesium atoms; respectively noted: 05Mg1100, 10Mg1100, 20Mg1100 and 50Mg1100 samples.

Furthermore, the pure hydroxyapatite samples (named the 00Mg series) of nominal composition $Ca_5(PO_4)_3{\cdot}OH$ and 5 at. % Mg-doped hydroxyapatite samples (named the 50Mg series) have been synthesised with calcinations temperature of 500, 700, 800, 900 and 1000°C. Samples are noted respectiveley 00Mg500, 00Mg700, 00Mg800, 00Mg900 and 00Mg1000 for the pure 00Mg series, and 50Mg500, 50Mg700, 50Mg800, 50Mg900 and 50Mg1000 for the 50Mg series.

The chemical compositions of all samples were determined by ICP-AES (Inductively Coupled Plasma-Atomic Emission Spectrometry). The nominal and experimental compositions of 00Mg series, 05Mg1100, 10Mg1100, 20Mg1100 and 50Mg series are listed in Table 1. As usually observed for sol-gel derived ceramics [40], the global nominal compositions have been achieved pretty well.

2.2 X-rays powder diffraction

Powder X-ray diffraction (PXRD) patterns were recorded on a X'Pert Pro Philips diffractometer, θ-θ geometry, equipped with a solid detector X-Celerator and using Cu K_α radiation (λ = 1.54184 Å). Powder pattern were recorded at room temperature in the interval $3° < 2\theta < 120°$, with a step size of $\Delta 2\theta$ = 0.0167° and a counting time of 200 s for each data value. A total counting time of about 200 min. was used for each sample. Si powder pattern was collected (from pure silicon standard) by using the same experimental conditions in order to extract the instrumental resolution function. The quality of the measured powder patterns with good statistic counting and good signal/background ratio allowed to perform quantitative Rietveld analyses by taking into account minor crystallized phases; i.e. below 1 weight % (wt. %).

2.3 Rietveld refinements

Powder pattern were analyzed by Rietveld refinement with *FullProf.2k* [41]. According to the calcination temperature and the Mg-doping level the following phases have been observed: hydroxyapatite (HAp), whitlockite (β-TCP), calcite $CaCO_3$, lime CaO, periclase MgO and the two dicalcium diphosphate polymorphs (α-$Ca_2P_2O_7$ and β-$Ca_2P_2O_7$). The initial structural parameters used for the Rietveld analyses were the following. The structural parameters of hydroxyapatite, $Ca_5(PO_4)_3{\cdot}OH$, were taken from [42]: space group $P6_3/m$, Z = 2, a = 9.4218 Å and c = 6.8813 Å, 7 independent atomic positions: two Ca, one P and four O positions. The O4 oxygen position (*i.e.* the hydroxyl anion) is half occupied, this corresponds to a statistically disordered 4*e* position shifted around the 2*a* (0,0,¼) site. The structural parameters of whitlockite, β-$Ca_3(PO_4)_2$, were taken from [43]: space group $R3c$, Z = 21, a = 10.4352 Å and c = 37.4029 Å, 18 independent atomic positions: five Ca, three P positions and ten O positions. The Ca5 calcium position has a partial occupancy factor. The structural parameters of lime, CaO (respectively periclase, MgO), were taken from [44] (respectively [45]): space group $Fm\bar{3}m$, Z = 4, a = 4.8071 Å (respectively a = 4.22 Å). The structural parameters of calcite, $CaCO_3$, were taken from [46]: space group $R\bar{3}c$, Z = 6, a = 4.9910 Å and c = 16.9719 Å. The structural parameters of α-$Ca_2P_2O_7$, were taken from [47]: space group $P2_1/n$, Z = 4, a = 12.66 Å, b = 8.542 Å, c = 5.315 Å and β = 90.3 °, 11 independent atomic positions: two Ca, two P positions and seven O positions. The structural parameters of β-$Ca_2P_2O_7$, were taken from [48]: space group $P4_1$, Z = 8, a = 6.6858 Å and c = 24.147 Å, 22 independent atomic positions: four Ca, four P positions and fourteen O positions. In a first step all the structural parameters were fixed to the literature values. Then during the

successive refinement cycles numerous parameters were allowed to vary accordingly to the relative weight amount of the observed phases. The following refinement sequence has been used: first lattice parameters, zero shift and peak profiles, and next atomic parameters: positional, isotropic temperature and occupancy factors. The scattering contrast between calcium and magnesium atoms allowed the refinement of the substitution by Mg in the different Ca sites for the main phases. The last refinement cycles were performed by introducing hydrogen atom from hydroxyl anion. The H4 (atom labels taken from [42] in all the text) position was located on the site 4*e*, a soft constraint of 0.92 ± 0.05 Å was applied to the distance O4-H4, and the isotropic temperature factors of H4 was constrained to be 1.2 times B_{iso} of the corresponding oxygen atom O4 as it is usual for hydroxyl groups [49-51]. The use of the instrumental resolution function improved the peak profile modelling while decreasing the number of profile parameters. It allowed also the extraction of the sample intrinsic microstructural parameters: average apparent crystallite size and average maximum strain. The diffraction profiles (both instrumental and sample intrinsic) were modelled by using a Thomson-Cox-Hastings pseudo-Voigt function [41]. Refinement with the anisotropic line broadening procedure [41] was used to calculate the anisotropy of morphology of the HAp crystallites. As indicated in [35] cares were taken to obtain accurate values for the quantitative phases analyses. An example of Rietveld plot can be found in supplementary information section for the 50Mg700 sample. Table 2 gathered the refined lattice parameters values of HAp and whitlockite, as well as the refined relative weight amount (wt. %) of the observed crystallised phases for each sample. Microstructural parameters of HAp, details on the localisation and the amount of Mg in the different Mg-doped samples and structural parameters of the Mg-doped β-TCP phases with composition $Ca_{2.841(9)}Mg_{0.159(9)}(PO_4)_2$ from the 50Mg1100 sample can be found as supplementary information (Table SI1 SI2 SI3 respectively).

2.4 Interaction with biological fluid

The Mg-substituted powdered samples (16 mg) were immersed at 37 °C for 1, 2, 5, 10 and 20 days in 24 ml of a standard Dulbecco's Modified Eagle Medium (DMEM; VWR International S.A.S., France); pH 7.3. DMEM contained the following mineral ingredients: NaCl (6400 $mg.l^{-1}$), KCl (400 $mg.l^{-1}$), $CaCl_2$ (200 $mg.l^{-1}$), $MgSO_4 \cdot 7H_2O$ (200 $mg.l^{-1}$), NaH_2PO_4 (124 $mg.l^{-1}$), $NaHCO_3$ (3700 $mg.l^{-1}$). DMEM has been considered rather than SBF because it matches more closely the biological conditions due in particular to the presence of amino acids. DMEM is also the culture medium that will be used for future cell interactions studies. At

each immersion time the concentration of the three elements Ca, P and Mg were determined by ICP-AES in the biological fluid after elimination of the solid by centrifugation.

3. Results and discussion

3.1 Effect of the temperature of calcination on the pure BCP series (i.e. the 00Mg series)

The PXRD patterns of the 00Mg series (i.e. samples 00Mg500, 00Mg700, 00Mg800, 00Mg900, 00Mg1000 and 00Mg1100) can be found as supplementary information (Figure SI2). All these powder patterns are mainly composed by the diffraction peaks of HAp phase (see stars in Figure SI2). Clear evidence of the increase of crystallinity when the temperature of calcinations increase is given by the evolution of the diffraction peak widths. The main phases are the expected HAp and β-TCP phases, and minor crystallised phases are α- and β-$Ca_2P_2O_7$, CaO and $CaCO_3$ (Table 2). In agreement with the literature the α-$Ca_2P_2O_7$ phase observed at 500°C and 700°C is transformed into the β-$Ca_2P_2O_7$ polymorph at 800°C (temperature of transition about 750°C) [47,48,52,53]. This dicalcium diphosphate phase disappeared at 1000°C. The calcite phase observed in the samples calcined at 500°C and 700°C disappeared in the sample calcined at 800°C and above, in agreement with its temperature of decomposition of the carbonate around 750°C [54]. The amount of lime (CaO) is dependent to the reactions transformation between the three phosphate phases: HAp (ratio Ca/P = 1.67), β-TCP (ratio Ca/P = 1.5) and $Ca_2P_2O_7$ (ratio Ca/P = 1.0). From 500°C to 900°C an increase of the lime wt. % is observed simultaneously with a decrease of the HAp wt. %, an increase of the β-TCP and $Ca_2P_2O_7$ wt. % and a disappearance of $CaCO_3$ due to the following reactions (Table 2 and Figure 1a):

$$2\ Ca_5(PO_4)_3OH \rightarrow 3\ Ca_3(PO_4)_2 + CaO + H_2O \quad (1)$$

$$2\ Ca_5(PO_4)_3OH \rightarrow 3\ Ca_2P_2O_7 + 4\ CaO + H_2O \quad (2)$$

$$CaCO_3 \rightarrow CaO + CO_2 \quad (3)$$

At 1000°C, and even more at 1100°C, a stabilisation of the HAp phase is observed (Figure 1a) simultaneously with an increase of the wt. % of CaO in disagreement with reactions (1) and (2). The increase of the CaO amount should be attributed either to the presence of an amorphous phase or to a non-stoechiometry of the HAp phase at high temperature. Refinements of the site occupancy factors for the calcium and hydroxide sites in HAp

structure did not evidenced a non-stoechiometry. All the refined occupancy parameters were very close to a full site filling, in agreement with the literature which indicates that HAp phase is stoechiometric (with a Ca/P ratio of 1.67) when calcined above the temperature of 700°C [10,31,32].

Lattice parameters of HAp and β-TCP are not temperature dependant (Table 2, Figure 1b). On the contrary, temperature dependence is observed for the anisotropy of the HAp crystallites morphology (Figure 1c), for the HAp and β-TCP coherent domain sizes and for HAp and β-TCP average maximum strains (Supplementary information Table SI1). Unit volumes per Ca atom are represented in Figure 1b in order to compare directly the behaviour of HAp (unit cell volume about 530 $Å^3$ with 10 Ca atoms per cell) and β-TCP (unit cell volume about 3530 $Å^3$ with 63 Ca atoms per cell) phases. The unit cell volume of the HAp heated at 500°C is quite larger (about 0.2 %) than the unit cell volumes measured for the HAp heated between 700°C to 1100°C (unit cell volume about 529.5 $Å^3$). The unit cell volumes of whitlockite (about 3531.1 $Å^3$, close to the published value of 3527.26 $Å^3$ [43]) is also invariant with the temperature of calcination. Upon heating an important increase of the coherent domain sizes (from about 500 Å at 500°C to more than 2000 Å at 1100°C) for both HAp and β-TCP phases and a clear decrease of the average maximum strains (from 2.0 ‰ at 500°C to 0.1 ‰ at 1100°C) for the HAp phase are observed. Microstrural parameters refinements indicate a needle-like morphology for the HAp crystals, elongated along the hexagonal axis (Figure 1c) as already mentioned [2]. The anisotropy of the HAp crystallite morpholohy decreases regularly when the temperature of calcination increases (Figure 1c). HAp crystallites become tabular above a calcinations temperature of 1000°C. The different crystallite morphologies of samples calcined at 500°C and 1100°C are shown in Figure 2.

3.2 Effect of the temperature of calcination on the 5% Mg-doped BCP series

Figure 3 displays a detail (two-theta range from 20° to 60°) of the PXRD patterns of the 50Mg series (i.e. samples 50Mg500, 50Mg700, 50Mg800, 50Mg900, 50Mg1000 and 50Mg1100). All these powder patterns are mainly composed by the diffraction peaks of HAp phase (see stars in Figure 3), except for the 50Mg1100 powder pattern in which the β-TCP contribution became predominant (see circles in Figure 3). As well as the pure BCP series, an increase of the crystallinity is observed when the temperature of calcinations increases. Minor crystallised phases are α- and β-$Ca_2P_2O_7$, CaO, $CaCO_3$, and also MgO which presents

relatively broad diffraction peaks (Table 2). The presence of magnesium in the sample seems not to affect the transition temperature from the α-$Ca_2P_2O_7$ to the β-$Ca_2P_2O_7$ polymorph which was still observed between 700°C and 800°C [47,48,52,53]. The amount of lime in the 50Mg series is clearly inferior to this observed previously in the pure BCP series. Lime is associated with a quite equivalent weight amount of periclase (MgO); i.e. around 1 wt. % for both alkaline earth oxide phases. Nevertheless we can observe a light increase of the weight amount of lime and periclase from 500°C to 800°C (same evolution already observed in the pure BCP series) following by a decrease of these weight amounts up to 1100°C (in contrast with the pure BCP series for which the weight amount of lime was maximal at 1100°C). The main difference observed between the two series (pure BCP and 50Mg series) is the clear stabilisation of the β-TCP phase in presence of magnesium at 1100°C. Between 500°C and 1000°C the two series show quite the same evolution of their quantitative phase analyses. And they completely invert the ratio HAp/β-TCP at 1100°C (Table 2 and Figure 1a). The stabilisation of the β-TCP phase do not correlates with the disappearance of lime at 1100°C, which disagrees again with the reaction (1). Then, the presence of amorphous phase, as identified in a previous study on Sr-doped HAp samples [35], should be considered. ICP-AES measurements indicate that the experimentally introduced MgO amounts agree with the expected nominal values (Tables 1 and 4). The total amounts of refined magnesium oxide (MgO from periclase and from the Mg substituted β-TCP phase) are also in quite good agreement with the expected nominal values for samples calcined at 1100°C (see supplementary informztion table SI2). Nevertheless, samples from the 50Mg series calcined at temperature below 900°C show a deficiency in the refined MgO amount proving the presence of an amorphous phase with a temperature dependant weight amount.

Refined lattice parameters (Table 2 and Figure 1b) indicate clearly that Mg insertion occurs in the β-TCP phase. The unit cell volume of β-TCP from the 50Mg1100 sample is about 3484.4 $Å^3$ (a decrease of 1.3 % compared to the value about 3531.1 $Å^3$ for the pure BCP series), close to the value of 3496.04 $Å^3$ for the referenced Mg-substituted whitlockite $Mg_{0.11}Ca_{2.89}(PO_4)_2$ [34]. The heating from 500°C to 900°C extracts Mg atoms from the whitlockite structure as showing by the increase of the corresponding unit cell volumes (from 3463.20 $Å^3$ at 500°C to 3483.14 $Å^3$ at 900°C) and the decrease of the refined Mg occupancies in Ca sites (x refined value from 0.23 at 700°C to 0.12 at 900°C in the $Ca_{3-x}Mg_x(PO_4)_2$ solid solution). The increase of the whitlockite unit cell mainly occurs above 700°C and is correlated with the evolution of the refined Mg amounts in Ca5 site in whitlockite structure (Supplementary information table

SI2 and Figure SI3). On the other hand the HAp unit cell volume did not show significant evolution when increasing the temperature of calcination. No difference is observed between the pure and the 50Mg series. The same unit cell volumes were observed for the HAp from the pure series (529.554 $Å^3$ when calcined at 1100°C) and the HAp from the 50Mg series (529.582 $Å^3$ when calcined at 1100°C). The only weak difference is observed for the temperature of calcinations of 500°C: HAp unit cell volume of 528.645 $Å^3$ in the 5%-Mg series and 530.500 $Å^3$ in the pure series. This decrease about 0.35% could indicate a small amount of Mg substitution in the HAp structure for 500°C calcination. At 700°C and above this small amount of substituted Mg atoms in the HAp phase is extracted (simultaneously with an increase of the crystallinity). The microstuctural parameters refined from the samples of this 50Mg series are related to those from the pure series; same order of crystallite size, crystal shape and average maximum strains (Figure 1c).

3.3 Effect of the Mg-doping amount in the BCP series calcined at 1100°C

Table 2 (and Figure SI4) show the evolution observed when introducing Mg atoms during the synthesis in our BCP samples. The known stabilisation effect of Mg on the β-TCP phase [10,29] is here clearly evidenced and characterized (Table 2 and Figure SI4a). The weight amount of β-TCP is quite linearly dependant to the amount of Mg atoms introduced during the synthesis (and inversely for HAp). A mixture of 50 wt. % of HAp - 50 wt. % of β-TCP is obtained for an introduced Mg about 3 at. %, whereas a quite pure HAp sample is formed when no Mg atoms are introduced. Evolution of the lattice parameters (Table 2 and Figure SI4b) indicates that Ca atoms are substituted by Mg in the β-TCP, and not in the HAp phase. More Mg atoms were introduced, more the unit cell volume of β-TCP decreased. Unit cell volume of the HAp phase is not sensitive to the introduction of Mg atoms during the synthesis. Figure 4 represents the Vegard's law relative to the $Ca_{3-x}Mg_x(PO_4)_2$ solid solution in the range $0.0 < x < 0.3$. This solid solution is limited (with $x < 1.5$) as showing by the monoclinic *C*2/*c* symmetry of the compound stanfieldite $Ca_{1.5}Mg_{1.5}(PO_4)_2$ [56]. The unit cell volume - refined composition ratio of our samples (stars in Figure 4) correlate fairly well with a linear Vegard's law fitted from the referenced values (circles and linear fit in Figure 4) [34,43]. Only the position of the sample 05Mg1100 diverges from the linear fit. No Mg atom was found in this sample during the Rietveld refinement, while the refined unit cell volume corresponds to a x value close to 0.03. This discrepency is attributed to the low amount of β-

TCP in the 05Mg1100 sample (i.e. less than 15 wt. %) leading to a not very stable refinement of its structural parameters.

3.4 Structural sites localization of Mg atoms in the BCP samples

During the last cycles of refinement attempts were performed to localize Mg atoms in all the Ca sites describing the HAp (two non-equivalent Ca sites represented in Figure 2 in [35]) and the β-TCP (five non-equivalent Ca sites represented in Figure SI3 in [35]). The seven possible sites were individually checked. The Mg occupancy factor was refined by constraining the alkaline earth full occupancy of the site (Mg occupancy + Ca occupancy = 1), except for the Ca4 site in whitlockite which present a half occupancy (Mg occupancy + Ca occupancy = ½). Whatever the sample, no Mg atoms were localized in the HAp phase; in perfect agreement with the observations on the lattice parameters (Figures 1b and SI4b). The structure of HAp heated at 1100°C is able to accept Ca substitution by a bigger alkaline earth as strontium [35,36], but not by a smaller alkaline earth as magnesium. The refined occupancies values for Mg in the Ca sites of the β-TCP phase can be found in supplementary information section (Table SI2). The Ca substitution by Mg is mainly realised in the Ca5 site (in agreement with [34]); in contrast with the substitution by Sr which occurs mainly in the Ca4 site [35,36]. Only the sample 50Mg1100 shows also a weak substitution of Ca by Mg in the Ca3 site. In contrast with the results given by [34,55] no indications were obtained concerning the substitution of Mg in the Ca4. The structural parameters of the Mg-doped withlockite phase with composition β-$Ca_{2.841(9)}Mg_{0.159(9)}(PO_4)_2$ from the 50Mg1100 sample can be found as supplementary information (Table SI3). A comparison of the Ca-O interatomic distance and the Bond Valence Sums (BVS) [57] for the five Ca sites for the pure β-TCP phase [43] and for β-$Ca_{2.841(9)}Mg_{0.159(9)}(PO_4)_2$ phase from the 50Mg1100 sample are given in supplementary information (Table SI4). Average interatomic distances and bond valences agree well with the non-substitution (or very weak substitution) by Mg in the sites Ca1, Ca2 and Ca3, as well as with the evident Mg substitution in the site Ca5. The half occupied Ca4 site is unusually coordinated to three oxygen atoms O9 belonging to the same phosphate (P1) tetrahedron (see the three broken bonds in the inset of Figure 4). A decrease of the average <Ca4-O> distances is observed, but is not provided by Mg substitution in this Ca4 site. The Ca5 has an octahedral coordination with no shared PO_4 edges (six neighbouring oxygen atoms belonging to six different PO_4 tetrahedra; see inset in Figure 4). Ca4 and Ca5 polyhedron form the low density column located on the threefold axis; as described and named the A column by Yashima et al.

[43]. Actually the insertion of Mg atoms in the Ca5 sites results in the deformation of the Ca4 polyhedron with a closeness of Ca4 and O9 atoms (broken bonds in the inset of Figure 4) which allows to increase the bond valence of the Ca4 site. BVS increases from 0.78 (pure β-TCP) to 1.29 (β-$Ca_{2.841(9)}Mg_{0.159(9)}(PO_4)_2$) for Ca4. A BVS value of 1.29 is still too weak for divalent cation, but widely better than 0.78. In the same time the BSV value of Ca5 site decrease from 2.73 (pure β-TCP) to 2.55 (β-$Ca_{2.841(9)}Mg_{0.159(9)}(PO_4)_2$). The doping stabilising feature of the whitlockite structure is realised by improving the inappropriate situation of the Ca4 environment; either by a direct substitution of a bigger alkaline earth (the case of Sr^{2+} cation which mainly substitute the Ca4 site [35]) or by a substitution of a smaller alkaline earth in the neighbouring Ca5 site of the low density column (the present case of Mg^{2+} which mainly substitute in the Ca5 site).

3.5 Interaction with biological fluid

The effects of the Mg-subtitution level (Figure 5) and the calcination temperature (Figure 6) on the interaction of BCP immersed in DMEM have been studied. The evolution of the Ca, Mg and P concentrations in DMEM give an indication of the dissolution of the BCP ceramic (i.e. increase of the concentrations in solution) and/or the precipitation at the surface of the BCP ceramic (i.e. decrease of the concentrations in solution). Figures 5 and 6 clearly show a precipitation of a calcium phosphate depicted by the decrease of [Ca] and [P] when the immersion time increases. On the other hand, the Mg concentration is quite invariable. The higher the Mg substitution level, the quicker the precipitation (Figure 5). For the 05MG1100, the concentrations of all cations are constant during the first ten days and the decrease of [Ca] and [P] are only observed after 20 days of immersion (Figure 5 top left). For the three other BCP ceramics calcined at 1100°C, the decrease of [Ca] and [P] are already observable for an immersion time of ten days. This gives indication of a kinetically favored precipitation of a calcium phosphate layer at the surface of the Mg-substituted samples. The presence of Mg in the BCP ceramics appears to be beneficial on the *in vitro* behavior. The dissolution of the immersed powder can also be observed by the weak increase of the Mg concentration for the high Mg content samples (Figure 5 bottom); i.e. for the samples with higher proportion of β-TCP and with the higher Mg content in the β-TCP phase. Despite the decrease of the solubility of whitlockite when increasing its magnesium content [37], in our all samples the Mg-substituted β-TCP phase has still a higher solubility than the HAp phase (as the maximal reached substitution corresponds to $Ca_{2.751(9)}Mg_{0.249(9)}(PO_4)_2$ composition). It has been already

mentioned that the *in vitro* bioactivity of HAp leads to the formation of a calcium phosphate layer which contains small amount of magnesium [38]. Then the presence of Mg element in the β-TCP phase of BCP powders seems to accelerate the precipitation of this layer. The effect of the calcination temperature (Figure 6) is correlated with the inserted Mg amount in the β-TCP phase. The Ca and P concentrations in DMEM are weaker after immersion of 50Mg700 compared to 50Mg500. And these concentrations are higher after immersion of 50Mg900 and even higher for 50Mg1100, compared to 50Mg700. This means that the precipitation of the calcium phophate layer is favoured at the surface of the 50Mg700 sample (i.e. the sample which contains the less soluble and the more stabilised Mg-substituted β-TCP phase). The solubility of the phases in BCP is not the most important feature to take into account to improve its bioactivity. The most important is the presence of nucleation sites at the crystallites surface which are activated by the presence of inserted magnesium atoms. The microstructural parameters, i.e. crystallinity and cristallite size, are certainly also important characteristics for the development of the biomimetic layer.

4. Conclusions

The sol-gel process has been used to prepare Mg-doped biphasic calcium phosphates (BCP) ceramics. With respect to un-substituted sample, the Mg-substituted samples exhibits higher proportion of β-TCP phase; namely at high temperature (above 1000°C). The Mg substitution in BCP ceramics concerns only the β-TCP phase. No Mg substitution has been observed in the HAp phase (or a very weak substitution when a moderate temperature of calcination, 500°C, is applied). The β-TCP weight amount in BCP is linearly dependant with the introduced Mg atomic amount for samples calcined at 1100°C. The Mg-substituted β-TCP cell parameters agree fairly well with the Vegard's law and Mg^{2+} ions substitute for Ca^{2+} only in the Ca5 site at low level of substitution. Such a stabilizing feature of Mg on the whitlockite structure is explained by an improvement of the environment of the Ca4 site. The Ca4 site, located on the three fold axis, is unusually face coordinated to a phosphate tetrahedron. Electrostatic repulsion increase the interatomic Ca4-O distances which leads to an extremely weak bond valence sum. The Mg substitution of the neighbouring Ca5 site allows to decrease these three larges Ca4-O bonds, which consequently leads to an improvment of the bond valence sums of both Ca4 and Ca5 sites. Such a stabilizing feature has been observed in the case of the Sr substitution. But in the Sr case, the substitution is directly realised in the

problematic Ca4 site because big cation accommodates well the large Ca4-O distances and improves directly its bond valence sum. From these results, it is clear that Mg substitution can be efficiently used to modulate the phase proportions of BCP and thus the behaviour in solution of the material. Interactions of our Mg-substituted BCP ceramics with DMEM have shown an accelerating effect of Mg on the precipitation of the calcium phosphate layer at the surface of the powder. A moderate temperature of calcination of 700°C led to the best bioactivity properties. The effective partial substitution of Mg in β-TCP makes this material very interesting for orthopaedic applications

Supporting Information Available:
Table SI1. Microstructural parameters refined for the hydroxyapatite (HAp) and whitlockite (β-TCP) phases.
Table SI2. Rietveld refinement results on the Mg insertion in the whitlockite structure.
Table SI3. Structural parameters of the Mg-doped withlockite phase with composition β-$Ca_{2.841(9)}Mg_{0.159(9)}(PO_4)_2$ from the 50Mg1100 sample.
Table SI4. Comparison of the interatomic distances and the calculated bond valence sum (BVS) for the pure and the Mg-doped with composition β-$Ca_{2.841(9)}Mg_{0.159(9)}(PO_4)_2$ from the 50Mg1100 sample.
Figure SI1. Rietveld plot on the 5% Mg-doped sample calcined at 700°C, 50Mg700 sample, (λ = 1.5418 Å).
Figure SI2. Details of the X-rays powder patterns (in the range $20 < 2\theta < 60°$) from the Mg free BCP series with calcination temperature from 500°C to 1100°C.
Figure SI3. Ca substitution level in the $Ca_{3-x}Mg_x(PO_4)_2$ solid solution for the 50Mg series and for the samples 20Mg1100 and 10Mg1100.
Figure SI4. Results of the Rietveld refinements as a function of the introduced Mg amount at 1100°C: quantitative phase analysis, unit volume per Ca = unit cell volume/unit cell number of Ca atoms.
This material is available free of charge via the Internet at http://pubs.acs.org.

Acknowledgements

Financial support from ANR under project Nanobonefiller (PNANO 2006) is gratefully acknowledged.

References

(1) Dahl, S. G.; Allain, P.; Marie, P. J.; Mauras, Y.; Boivin, G.; Ammann, P.; Tsouderos, Y.; Delmas, P. D.; Christiansen, C. *Bone* **2001**, *28*, 446.

(2) Lagier, R.; Baud, C. -A. *Pathol. Res. Pract.*, **2003,** *199*, 329.

(3) Lee, R. S.; Kayser, M. V.; Ali, S. Y. *J. Anat.* **200**6, *208*, 13.

(4) Elliot, J. C. *Structure and Chemistry of the Apatites and Other Calcium Orthophosphates*, Elsevier, Amsterdam, The Netherlands, 1994.

(5) LeGeros, R. Z.; Lin, S.; Rohanizadeh, R.; Mijares, D.; LeGeros, J. P. *J. Mater. Sci. Mater. Med.* **2003**, *14*, 201.

(6) Livingston Arinzeh, T.; Tran, T.; Mcalary, J.; Daculsi, G. *Biomaterials* **2005,** *26*, 3631.

(7) Bouler, J. M.; Trecant, M.; Delecrin, J., Royer, J.; Passuti, N.; Daculsi, G. *J. Biomed. Mater. Res.* 1996, *32*, 603.

(8) Ergun, C.; Webster, T. J.; Bizias, R.; Doremus, R. H. *J. Biomed. Mater. Res*. 2002, *59*, 305.

(9) Creedon, A.; Flynm, A.; Cashman, A. *Br. J. Nutr*. 1999, *82*, 63.

(10) Kannan, S.; Lemos, I. A. F; Rocha, J. H. G; Ferreira, J. M. F. *J. Sol. State chem*. **2005**, *178*, 3190.

(11) Rude, R. K. *J. Bone Miner. Res.* **1998**, *13*, 749.

(12) Serre, C. M.; Papillard, M.; Chavassieux, P.; Voegel, J. C.; Boivin G. *J. Biomed. Mater. Res.*, **1998**, *42*, 626.

(13) Tsuboi, S.; Nakagaki, H.; Ishiguro, K.; Kondo, K.; Mukai, M.; Robinson, C.; Weatherell, J. A. *Calcif. Tissue Int.* **1992**, *50*, 34.

(14) Fondel, C.; Prien, E. L. *Science* **1946**, *103*, 326.

(15) Jensen, A. T.; Rowles, S. L. *Acta Odont. Scand.* **1957**, *16*, 121.

(16) LeGeros, R. Z. ; LeGeros, J. P. Phosphate minerals in human tissues, in *Phosphate minerals*, Nriagu, J. O. and Moore, P. B. Eds., Springer, Heidelberg, Berlin, pp 351-355.

(17) Ryan, L. M.; Cheung, H. S.; LeGeros, R. Z.; Kurup, I. V.; Toth, J.; Westfall, P. R.; Mc Carthy, G. M. *Calcif. Tissue Int.* **1999** , *65*, 374.

(18) Klein, C. P. A. T.; Driessen, A. A.; De Groot, K. *J. Biomed. Mater. Res*. **1983**, *17*, 769.

(19) Klein, C. P. A. T.; De Groot, K.; Driessen, A. A; Van der Lubbe, H. B. M. *Biomaterial*s, **1986**, *7*, 144.

(20) Dhert, W. J. A.; Klein, C. P. A. T.; Jansen, J. A.; Van der Velde, E. A.; Vriesde, R. C.; Rozing, P. M.; De Groot, K. *J. Biomed. Mater. Res.* **1993**, *27*, 127.

(21) LeGeros, R. Z.; Daculsi, G.; Kijkowska, R.; Kerebel, B. The effect of magnesium on the formation of apatites and withlockites, in *Magnesium in Health and Disease*, Itokawa Y. and Durlach J. Eds., John Libbey and Co., Ltd., New York, 1989.

(22) Bigi, A.; Foresti, E.; Gregorini, R.; Ripamonti, A.; Roveri, N.; Shah, J. S. *Calcif. Tissue Int.* **1992**, *50*, 439.

(23) Boskey, A. L.; Rimnac, C. M.; Bansal, M.; Federmann, M.; Lian J.; Boyan, B. D. *J. Orthop. Res* **1992**, *10*, 774.

(24) Montel, G.; Bonel, G.; Heughebaert, J. C.; Trombe, J. C.; Rey, C. *J. Crystal Growth* **1981**, *53*, 74.

(25) Hamad, M.; Heughebaert, J. C.; *J. Crystal Growth* **1986**, *79*, 192.

(26) Hamad, M.; Heughebaert, J. C. *J. Chim. Phys.* **1987**, *84*, 985.

(27) Ben Abdelkader, S.; Khattech, I.; Rey, C.; Jemal, M. *Thermochimica Acta* **2001**, *376*, 25.

(28) Suchanek, W. L.; Byrappa, K.; Shuk, P.; Riman, R. E.; Janas, V. F.; Ten Huisen, K. S. *Biomaterials* **2004**, *25*, 4647.

(29) Gibson, I. R.; Bonfield, W. *J. Mater. Sci. Mater. Med.* **2002**, *13*, 685.

(30) Fadeev, I. V.; Shorneva, L. I.; Barinov, S. M.; Orlovskii, V. P. *Inorg. Mater*. **2003**, *39*, 947.

(31) LeGeros, R. Z., Calcium phosphates in oral biology and medicine in *Monographs in Oral Science*, Karger, Basel, Myers, H. M., Ed. 1991, *15*.

(32) Ishikawa, K.; Ducheyne, P.; Radin, S. *J. Mater. Sci. Mater. Med*. **1993**, *4*, 165.

(33) Dickens, B.; Schroeder, L. W.; Brown, W. E. J. *Sol. State Chem.* **1974**, *10*, 232.

(34) Schroeder, L. W.; Dickens, B.; Brown, W. E. *J. Sol. State Chem*. **1977**, *22*, 253.

(35) Renaudin, G.; Laquerrière, P.; Filinchuk, Y.; Jallot, E.; Nedelec, J.M. *J. Mater. Chem.* **2008**, *18*, 3593.

(36) Renaudin, G., Jallot, E.; Nedelec, J.M. *J. Sol-Gel Science and Technology*, in press.

(37) Li, Xia ; Ito, Atsuo; Sogo, Yu; Wang, Xiupeng; LeGeros, R.Z. *Acta Biomater* **2009**, *5*,508.

(38) Jallot, E.; Nedelec, J.M.; Grimault, A.S., Chassot, E.; Laquerriere, P.; Grandjean-Laquerriere, A.; Laurent-Maquin, D. *Colloids and Surface* **2005**, *B 42*, 205.

(39) Grandjean-Laquerriere, A.; Laquerriere, P.; Jallot, E.; Nedelec, J.M.; Guenounou, M.; Laurent-Maquin, D.; Philips, T. *Biomaterials* **2006**, *27*, 3195.

(40) Nedelec, J.M.; Courtheoux, L.; Jallot, E.; Lao J.; Kinowski, C.; Laquerriere, P.; Mansuy, C.; Renaudin, G.; Turrell, S. *J. Sol-Gel Science and Technology* **2008** , *46*, 259.

(41) Rodriguez-Carvajal, J. PROGRA*M FullProf.2k* – version 3.20; Laboratoire Léon Brillouin (CEA-CNRS); France; **200**5 (FullProf.2k manual available on http://www-llb.cea.fr/fullweb/fp2k/fp2k_divers.htm). See also Rodriguez-Carvajal, J.; Roisnel, T. *EPDIC-8*, Uppsala, Sweden, May 23-26, 2002*;* Trans. Tech. Publication Ltd, Materials Science Forum 123, 2004; 443.

(42) Rodriguez-Lorenzo, L. M.; Hart, J. N.; Gross, K. A. *J. Phys. Chem. B.* **2003**, *107*, 8316.

(43) Yashima, M.; Sakai, A.; Kamiyama, T.; Hoshikawa, A. *J. Solid State Chem*. **2003**, *175,* 272.

(44) Ganguly, R.; Siruguri, V.; Gopalakrishnan, I. K.; Yakhmi, J. V. *J. Phys.: Condensed Matter* **2000**, *12*, 1283.

(45) Bragg, W. L. Nature **1920,** *105*, 646.

(46) Chessin, H.; Hamilton, W. C. ; Post B. *Acta Cryst.* **1965**, *18*, 689.

(47) Calvo, C. *Inorg. Chem.* **1968**, *7*, 1345.

(48) Boudin, S.; Grandin, A.; Borel, M. M.; Leclaire, A. ; Raveau, B. Acta Cryst. ***1993***, *C49*, 2062.

(49) François, M.; Renaudin, G. ; Evrard, O. *Acta Cryst*. **1998**, *C54* , 1214.

(50) Renaudin, G. ; François, M. *Acta Cryst.* **1999**, *C55*, 835.

(51) Renaudin, G.; Rapin, J.-P.; Humbert, B.; François, M. *Cem. Concr. Res.* **2000**, *30*, 307.

(52) Parodi, J. A.; Hickok, R. L.; Segelken, W. G.; Cooper, J. R. *J. Electrochem. Soc.* **1965** *112*, 688.

(53) Bian, J.-J.; Kim, D.-W.; Hong, K.-S. *Mat. Let.* **2004**, *58*, 347.

(54) Renaudin, G.; Bertrand, A.; Dubois, M.; Gomes, S.; Chevalier, P. ; Labrosse, A. *J. Phys. Chem. Sol.* **2008**, *69*, 1603.

(55) Bigi, A.; Falini, G.; Foresti, E.; Ripamonti, A.; Gazzano, M., Roveri, N. *Zeit. Krist.* **1996**, *211*, 13.

(56) Dickens, B.; Brown, W. E. *Tschermaks Mineralogische und Petrographische Mitteilungen 1971* , *16*, 79.

(57) Brese, N. E.; O'Keefe M. *Acta Cryst.* **1991**, B47, 192.

Table 1. Nominal and experimental (determined by ICP-AES) composition (wt %) of Ca, P and Mg in the synthesised samples.

Samples	Nominal composition				Experimental composition			
	Ca	P	Mg	Substitution level (%)	Ca	P	Mg	Substitution level (%)
00Mg series	39.90	18.50	0	0	41.89	18.05	0	0
05Mg1100	39.73	18.51	0.12	0.50	40.48	18.83	0.13	0.52
10Mg1100	39.56	18.53	0.24	1.00	40.24	18.89	0.25	1.03
20Mg1100	39.22	18.56	0.49	2.00	40.27	18.70	0.49	1.97
50Mg series	38.20	18.65	1.22	5.00	38.08	19.55	1.16	4.77

Table 2. Results of the quantitative phase analyses using the Rietveld method, and refined lattice parameter of the hydroxyapatite (HAp) and whitlockite (β-TCP) phases. Standard deviations are indicated in parentheses.

Sample			HAp			β-TCP			α-$Ca_2P_2O_7$	β-$Ca_2P_2O_7$	CaO	$CaCO_3$	MgO
Label	Mg [a] at. %	T (°C)	wt. % [b]	*a* (Å)	*c* (Å)	wt. % [b]	*a* (Å)	*c* (Å)	wt. % [b]	wt.% [b]	wt. % [b]	wt. % [b]	wt. % [b]
00Mg500	0.0	500	93.0(2)	9.43471(9)	6.88173(9)	-	-	-	2.88 (4)	-	2.35(2)	1.79(3)	-
00Mg700	0.0	700	84.7(2)	9.42210(8)	6.88582(6)	3.27(6)	10.4412(5)	37.419(2)	8.47 (9)	-	2.86(2)	0.73(2)	-
00Mg800	0.0	800	82.0(2)	9.42327(4)	6.88490(3)	9.8(1)	10.4408(2)	37.4106(7)	-	3.13(6)	5.08(4)	-	-
00Mg900	0.0	900	71.6(2)	9.42376(3)	6.88367(3)	24.0(1)	10.44016(9)	37.4007(4)	-	0.65(6)	3.69(2)	-	-
00Mg1000	0.0	1000	75.7(2)	9.42461(1)	6.88415(2)	20.2(2)	10.4403(1)	37.4033(5)	-	-	4.10(3)	-	-
00Mg1100	0.0	1100	91.7(2)	9.42454(2)	6.88429(2)	1.11(4)	10.4412(5)	37.401(3)	-	-	7.14(3)	-	-
05Mg1100	0.5	1100	87.3(3)	9.42456(2)	6.88434(2)	12.2(2)	10.4241(2)	37.3883(9)	-	-	0.39(2)	-	0.11(2)
10Mg1100	1.0	1100	76.4(2)	9.42414(2)	6.88448(2)	22.4(2)	10.4218(1)	37.3775(4)	-	-	0.89(2)	-	0.28(2)
20Mg1100	2.0	1100	63.1(2)	9.42447(2)	6.88450(2)	35.2(2)	10.41224(7)	37.3643(3)	-	-	1.21(2)	-	0.46(2)
50Mg500	5.0	500	84.6(3)	9.41791(8)	6.88214(7)	13.2(1)	10.3653(5)	37.220(2)	-	-	0.34(2)	1.00(4)	0.89(3)
50Mg700	5.0	700	77.3(2)	9.42316(7)	6.88619(6)	16.1(1)	10.3642(4)	37.231(2)	5.04(6)	-	0.55(1)	0.66(3)	0.36(2)
50Mg800	5.0	800	75.8(2)	9.42390(4)	6.88600(3)	16.1(1)	10.3745(2)	37.2874(8)	-	6.11(6)	0.82(1)	-	1.15(2)
50Mg900	5.0	900	60.6(2)	9.42558(3)	6.88615(3)	37.0(1)	10.38257(7)	37.3107(3)	-	0.87(5)	0.47(1)	-	1.03(2)
50Mg1000	5.0	1000	67.8(2)	9.42521(3)	6.88578(2)	29.9(1)	10.38702(8)	37.2930(4)	-	0.47(5)	0.48(2)	-	1.34(3)
50Mg1100	5.0	1100	30.0(1)	9.42402(4)	6.88541(3)	69.5(2)	10.38506(6)	37.3060(3)	-	-	-	-	0.46(2)

[a] the Mg at. % value corresponds to the calcium atomic percent substituted by magnesium.
[b] weight percent.

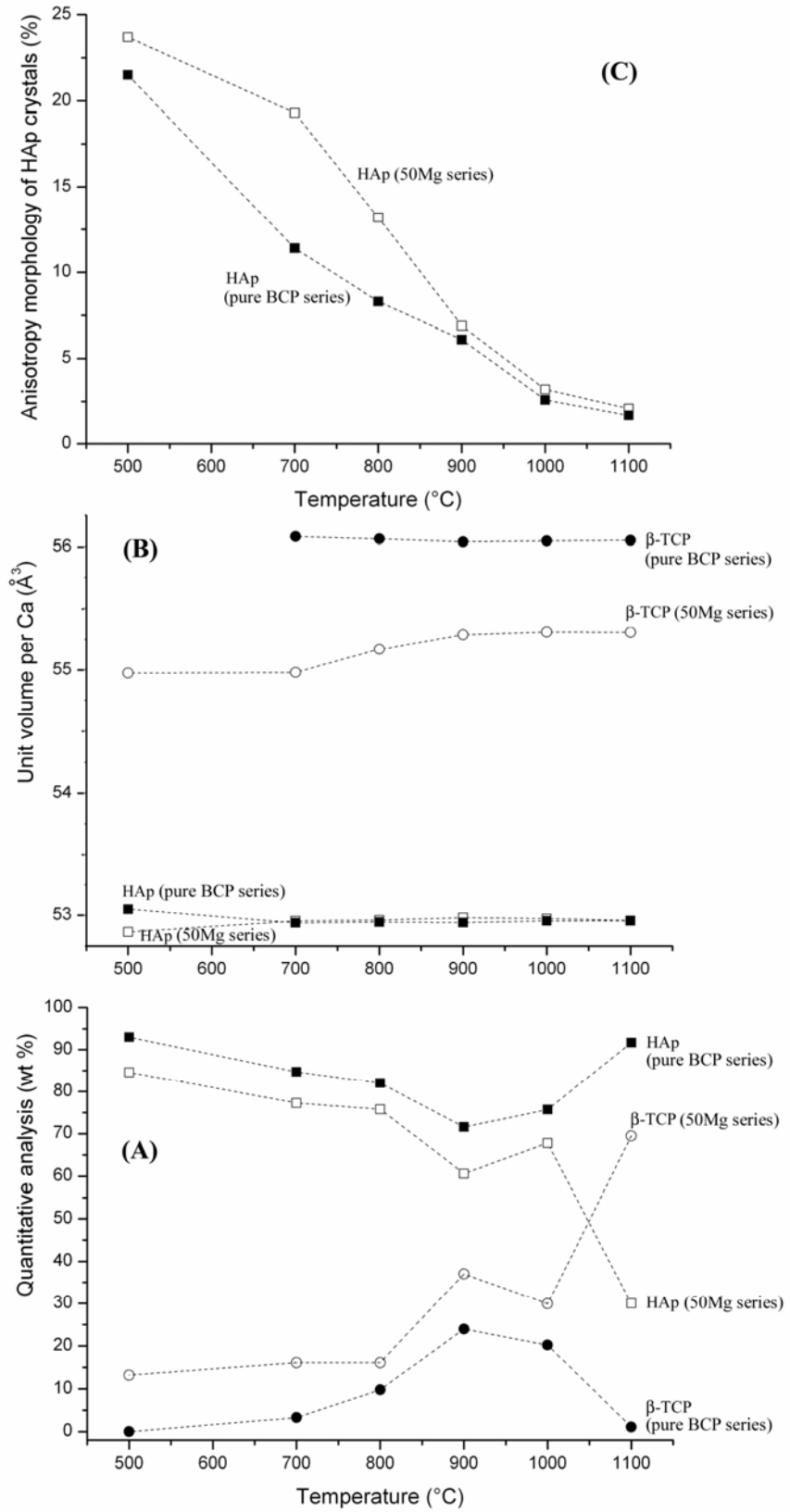

Figure 1. Rietveld refinements results as a function of the temperature: (A) quantitative phase analysis, (B) unit volume per Ca = unit cell volume/number of Ca atoms per cell, (C) anisotropy of the hydroxyapatite crystal morphology = ($Lc_{[110]}$ – $Lc_{[001]}$)/2<Lc>*100 (Lc: coherent domain length, see Table SI1). Results are represented for the HAp phase (squares) and the β-TCP phase (circles). Filled (respectively opened) symbols are relative to the pure BCP series (respectively 5% Mg-doped BCP series). Dashed lines are only guides for eyes.

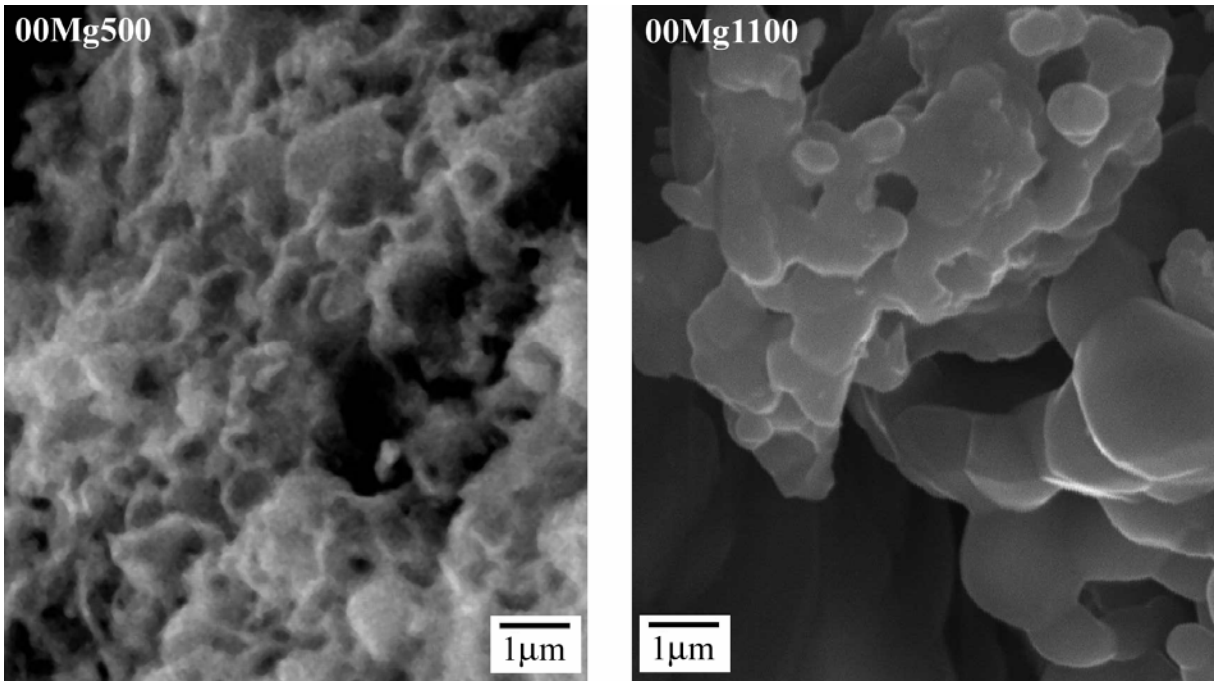

Figure 2. Representative SEM images of Mg free sol-gel BCP samples calcined at 500°C (left) and 1100°C (right).

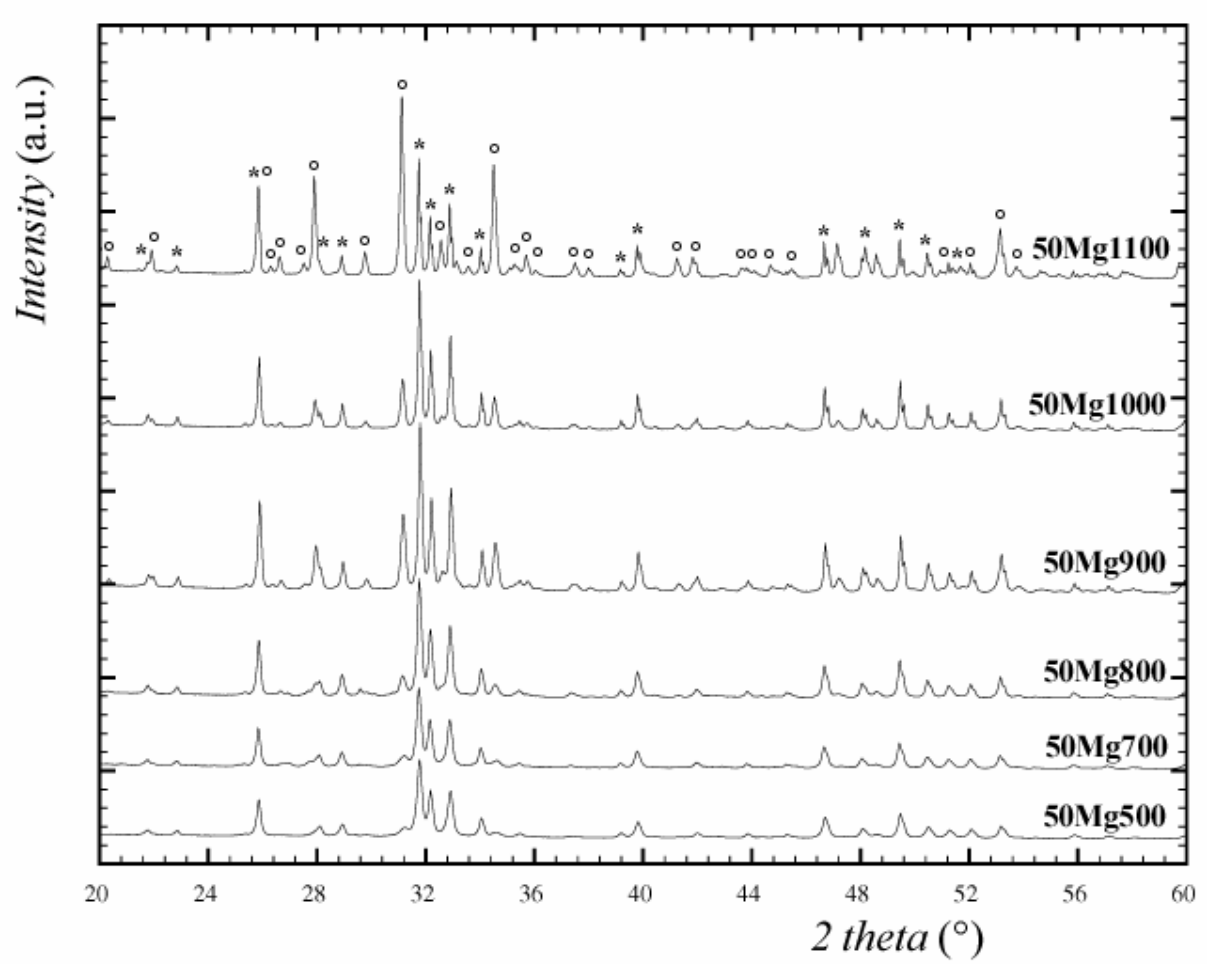

Figure 3. Details of the X-rays powder patterns (in the range $20 < 2\theta < 60°$) from the 50Mg series with calcination temperature from 500°C to 1100°C. The marks ***** and **°** indicate respectively the main diffraction peaks of hydroxyapatite (HAp) and whitlockite (β-TCP) phases.

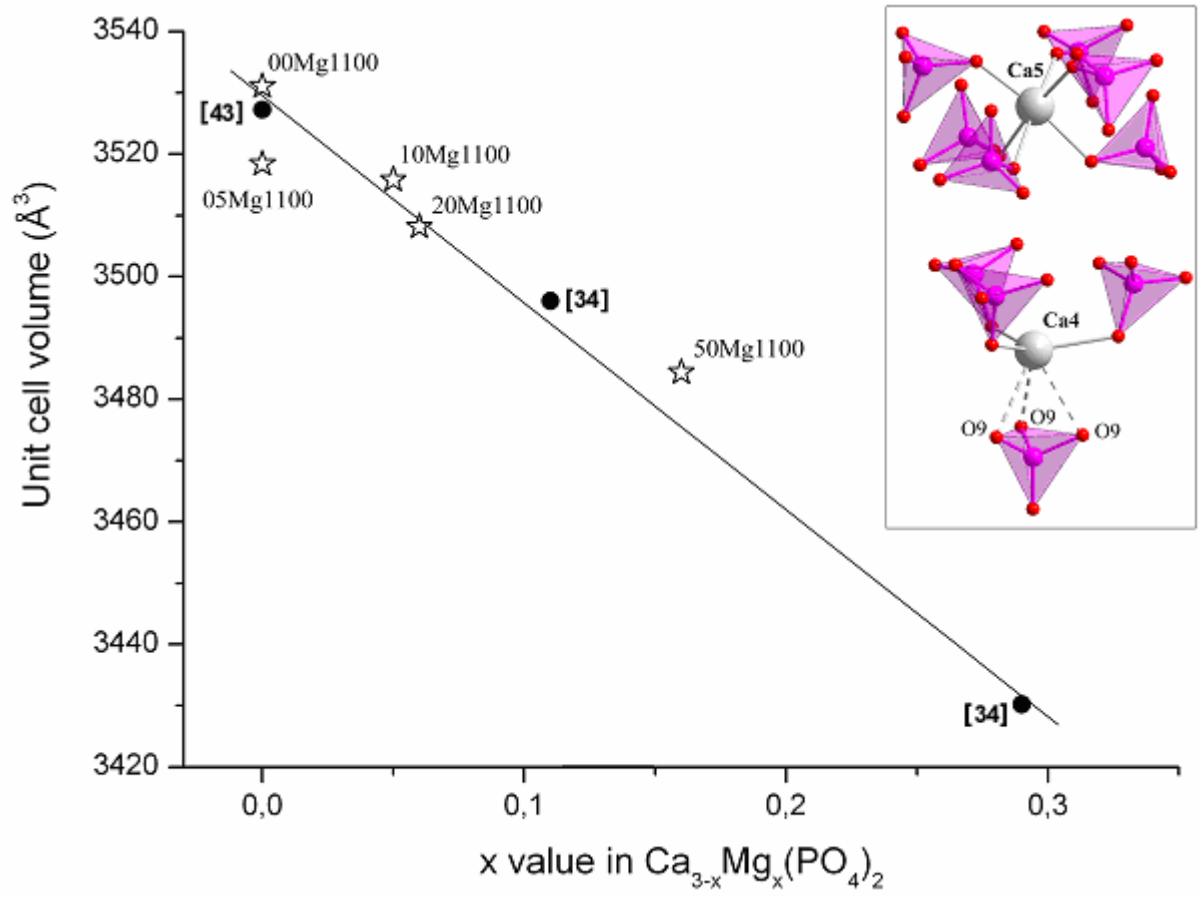

Figure 4. Representation of the Vegard's law for the $Ca_{3-x}Mg_x(PO_4)_2$ solid solution for $0.0 < x < 0.3$. Close circles, with the corresponding linear fit correspond to the literature values ([43] for x = 0.0, [34] for x = 0.11 and 0.29). Open stars, with corresponding sample labels, are values from the present works. Details of the structure of $Ca_{3-x}Mg_x(PO_4)_2$ compound is drawing in the inset, with the substituted Ca5 site allowing the crystallographic stabilisation of the neighbouring Ca4 site.

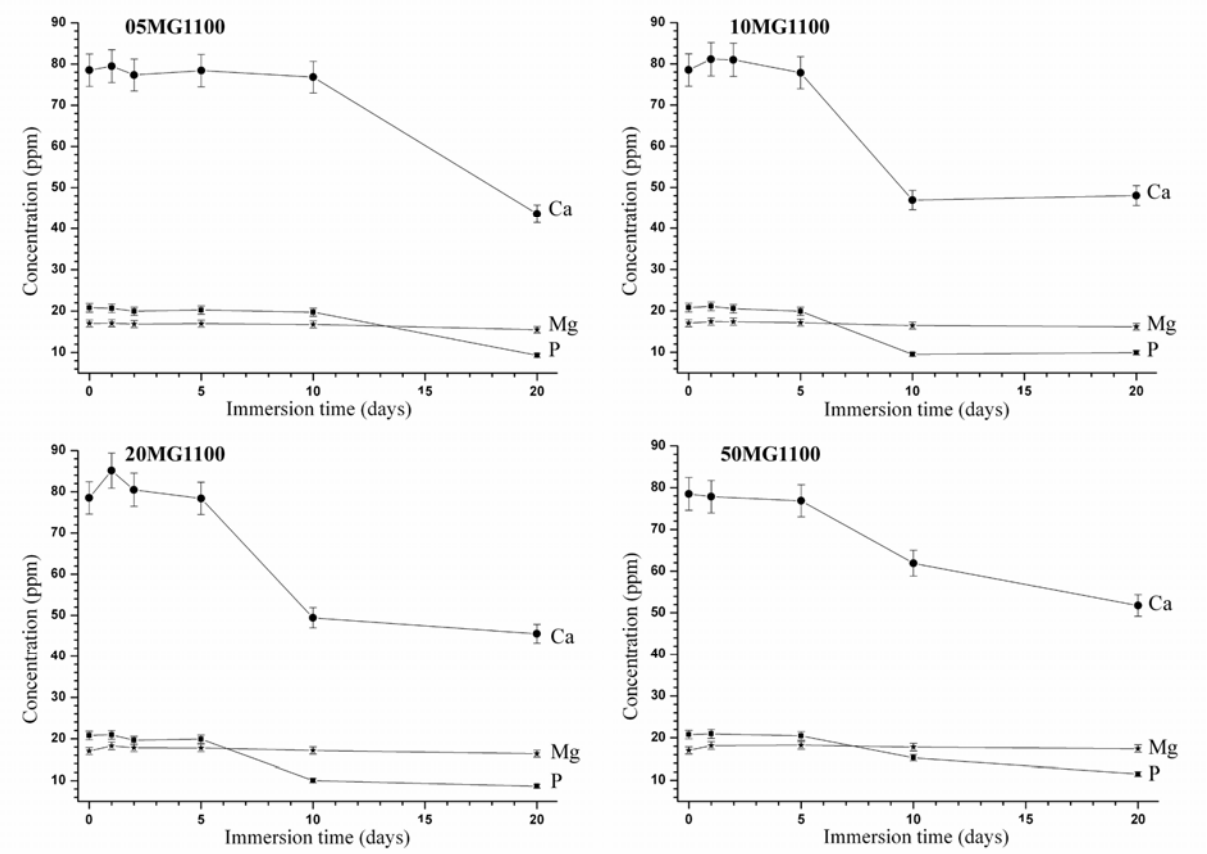

Figure 5. Evolution of the Ca (circles), Mg (stars) and P (squares) concentrations of the DMEM after immersion of the four Mg-substituted powdered samples calcined at 1100°C.

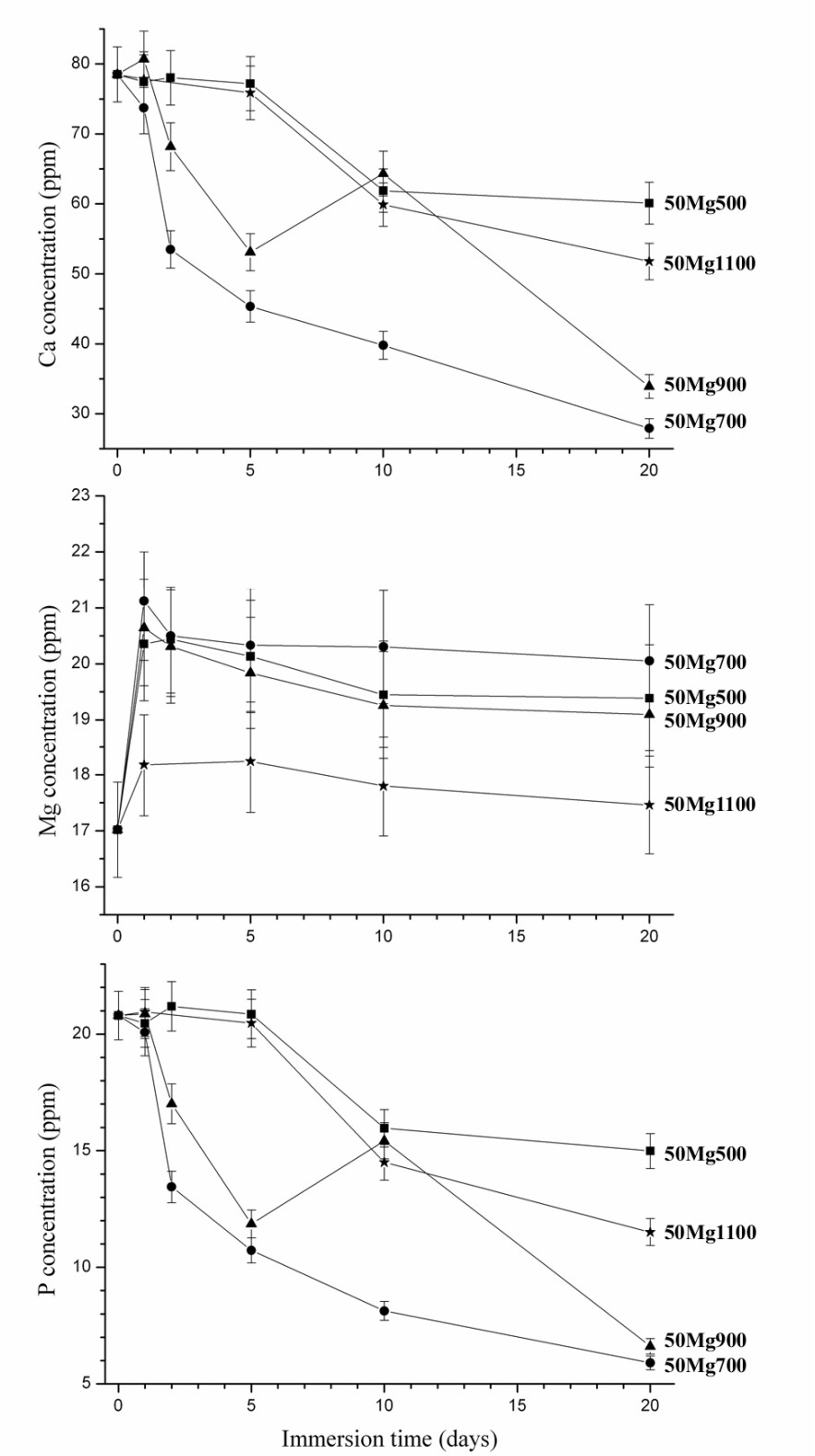

Figure 6. Evolution of the Ca (top), Mg (middle) and P (bottom) concentrations of the DMEM after immersion of the 5 at. % of Mg-substituted powdered samples calcined at 500 (squares), 700 (circles), 900°C (triangles) and 1100°C (stars).

Supporting Information Available:

Table SI1. Microstructural parameters refined for the hydroxyapatite (HAp) and whitlockite (β-TCP) phases. Standard deviations are indicated in parentheses.

Sample	HAp					β-TCP	
	$Lc_{[110]}$ [a] (Å)	$Lc_{[001]}$ [a] (Å)	<Lc> [b] (Å)	Aniso. [c] (%)	Strain [e] (‰)	Lc [d] (Å)	Strain [e] (‰)
00Mg500	290	445	360	21.5	2.00(1)	-	-
00Mg700	445	555	480	11.4	0.88(1)	560(10)	0.65(1)
00Mg800	700	825	750	8.3	0.36(1)	1080(10)	0.75(1)
00Mg900	1120	1265	1190	6.1	0.19(1)	1630(10)	0.86(1)
00Mg1000	1625	1715	1700	2.6	0.09(1)	1704(10)	0.87(1)
00Mg1100	2260	2340	2300	1.7	0.14(1)	2250(10)	0.05(1)
50Mg500	480	755	580	23.7	0.75(1)	430(10)	4.56(1)
50Mg700	525	760	610	19.3	0.62(1)	910(10)	4.95(1)
50Mg800	680	875	740	13.2	0.37(1)	870(10)	2.98(1)
50Mg900	1105	1270	1200	6.9	0.23(1)	1110(10)	1.95(1)
50Mg1000	1770	1890	1850	3.2	0.25(1)	1470(10)	1.51(1)
50Mg1100	2560	2670	2620	2.1	0.23(1)	1630(10)	1.02(1)

[a] coherent domain length along the corresponding [*uvw*] direction.
[b] average coherent domain size for anisotropic crystals.
[c] crystal morphology anisotropy = $(Lc_{[110]} - Lc_{[001]})/2<Lc>*100$.
[d] coherent domain size for isotropic crystals.
[e] average maximum strain (isotropic model).

Table SI2. Rietveld refinement results on the Mg insertion in the whitlockite structure. Standard deviations are indicated in parentheses.

Sample	MgO (wt. %)		β-TCP				MgO refined [c] (wt. %)
	Nominal [a]	ICP [b]	Mg occupancies Ca3	Mg occupancies Ca5	Mg (at.%)	Refined composition	
05Mg1100	0.20	0.21(1)	-	-	0.0(-)	$Ca_3(PO_4)_2$	0.11(2)
10Mg1100	0.40	0.42(2)	-	0.18(3)	1.7(3)	$Ca_{2.949(9)}Mg_{0.051(9)}(PO_4)_2$	0.43(2)
20Mg1100	0.80	0.81(4)	-	0.21(2)	2.0(2)	$Ca_{2.940(6)}Mg_{0.060(6)}(PO_4)_2$	0.74(2)
50Mg1100	2.02	1.9(1)	0.033(9)	0.46(1)	5.3(3)	$Ca_{2.841(9)}Mg_{0.159(9)}(PO_4)_2$	1.91(2)
50Mg1000	2.02	1.9(1)	-	0.44(2)	4.2(2)	$Ca_{2.874(6)}Mg_{0.126(6)}(PO_4)_2$	1.83(2)
50Mg900	2.02	1.9(1)	-	0.41(2)	3.9(2)	$Ca_{2.883(6)}Mg_{0.117(6)}(PO_4)_2$	1.60(2)
50Mg800	2.02	1.9(1)	-	0.39(3)	3.7(3)	$Ca_{2.889(9)}Mg_{0.111(9)}(PO_4)_2$	1.42(2)
50Mg700	2.02	1.9(1)	-	0.87(3)	8.3(3)	$Ca_{2.751(9)}Mg_{0.249(9)}(PO_4)_2$	0.89(2)
50Mg500	2.02	1.9(1)	-	0.81(5)	7.7(6)	$Ca_{2.77(2)}Mg_{0.23(2)}(PO_4)_2$	1.29(3)

[a] Theoretical MgO weight % in the whole sample introduced during the synthesis process.
[b] MgO weight % in the whole sample measured by ICP-AES analyses.
[c] Total elementary magnesium oxide (contained in periclase and Mg-substituted whitlockite phases) from Rietveld refinements.

Table SI3. Structural parameters of the Mg-doped withlockite phase with composition β-$Ca_{2.841(9)}Mg_{0.159(9)}(PO_4)_2$ from the 50Mg1100 sample. Standard deviations are indicated in parentheses.

Phase	Atom	Site	*x*	*y*	*z*	B_{iso} (Å^2)	Occ.[b]
$Ca_{2.841(9)}Mg_{0.159(9)}(PO_4)_2$	Ca1	18*b*	0.7250(3)	0.8548(5)	0.1675(2)	0.87(2)	1(-)
*R*3*c*, Z = 21	Ca2	18*b*	0.6176(3)	0.8205(5)	-0.0330(2)	= $B_{(Ca1)}$	1(-)
a = 10.38506(6) Å	Ca3	18*b*	0.7281(3)	0.8520(4)	0.0612(2)	= $B_{(Ca1)}$	0.967(9)
c = 37.3060(3) Å	Mg3	18*b*	= $x_{(Ca3)}$	= $y_{(Ca3)}$	= $z_{(Ca3)}$	= $B_{(Ca1)}$	= 1-$Occ_{(Ca3)}$
R_{Bragg} = 0.024	Ca4	6*a*	0	0	-0.0810(3)	= $B_{(Ca1)}$	0.5(-)
*R*p = 0.030	Ca5	6*a*	0	0	0.7340(2)	= $B_{(Ca1)}$	0.54(1)
*R*wp = 0.040	Mg5	6*a*	= $x_{(Ca5)}$	= $y_{(Ca5)}$	= $z_{(Ca5)}$	= $B_{(Ca1)}$	= 1-$Occ_{(Ca5)}$
	P1	6*a*	0	0	0(-)	1.05(4)	1(-)
	P2	18*b*	0.6872(4)	0.8605(6)	0.8692(2)	= $B_{(P1)}$	1(-)
	P3	18*b*	0.6540(5)	0.8474(6)	0.7662(2)	= $B_{(P1)}$	1(-)
	O1	18*b*	0.7411(8)	-0.0870(8)	-0.0919(3)	0.50(4)	1(-)
	O2	18*b*	0.769(1)	0.778(1)	0.8578(3)	= $B_{(O1)}$	1(-)
	O3	18*b*	0.724(1)	0.006(1)	0.8484(3)	= $B_{(O1)}$	1(-)
	O4	18*b*	0.5196(8)	0.766(1)	0.8660(3)	= $B_{(O1)}$	1(-)
	O5	18*b*	0.604(1)	-0.046(1)	0.7804(3)	= $B_{(O1)}$	1(-)
	O6	18*b*	0.577(1)	0.695(1)	0.7865(3)	= $B_{(O1)}$	1(-)
	O7	18*b*	0.082(1)	0.904(1)	0.7764(3)	= $B_{(O1)}$	1(-)
	O8	18*b*	0.6287(7)	0.8282(9)	0.7271(3)	= $B_{(O1)}$	1(-)
	O9	18*b*	0.0086(9)	0.8660(6)	-0.0182(3)	= $B_{(O1)}$	1(-)
	O10	6*a*	0	0	0.0394(4)	= $B_{(O1)}$	1(-)

Table SI4. Comparison of the interatomic distances and the calculated bond valence sum (BVS) for the pure and the Mg-doped with composition β-$Ca_{2.841(9)}Mg_{0.159(9)}(PO_4)_2$ from the 50Mg1100 sample. Standard deviations are indicated in parentheses.

	Pure β-TCP [33]			Mg-doped β-TCP from 50Mg1100		
	polyhedra	distance (Å)	BVS	polyhedra	distance (Å)	BVS
Ca1 (CN8)	O6	2.327(7)	0.38	O6	2.29(1)	0.42
	O5	2.390(7)	0.32	O8	2.39(1)	0.32
	O8	2.419(6)	0.29	O5	2.45(1)	0.27
	O4	2.451(8)	0.27	O4	2.48(1)	0.25
	O9	2.464(8)	0.26	O4	2.49(1)	0.24
	O4	2.471(8)	0.26	O3	2.50(1)	0.24
	O3	2.512(7)	0.23	O9	2.524(8)	0.22
	O2	3.001(8)	0.06	O2	2.94(1)	0.07
	<Ca1-O>	**2.50**	**2.07**	<Ca1-O>	**2.51**	**2.03**
Ca2 (CN8)	O9	2.357(8)	0.35	O9	2.288(8)	0.42
	O3	2.375(7)	0.33	O3	2.35(1)	0.36
	O1	2.406(7)	0.31	O7	2.41(1)	0.30
	O2	2.419(7)	0.29	O7	2.41(1)	0.30
	O7	2.422(8)	0.29	O1	2.48(1)	0.25
	O7	2.424(7)	0.29	O2	2.48(1)	0.25
	O5	2.702(7)	0.14	O5	2.60(1)	0.18
	O6	2.744(8)	0.12	O6	2.74(1)	0.12
	<Ca2-O>	**2.48**	**2.12**	<Ca2-O>	**2.47**	**2.18**
Ca3 (CN8)	O3	2.354(7)	0.35	O3	2.37(1)	0.33
	O5	2.393(6)	0.32	O5	2.44(1)	0.27
	O6	2.547(7)	0.21	O2	2.49(1)	0.24
	O8	2.568(7)	0.20	O8	2.555(9)	0.20
	O10	2.573(4)	0.19	O8	2.57(1)	0.19
	O2	2.599(7)	0.18	O10	2.580(6)	0.19
	O8	2.622(7)	0.17	O6	2.59(1)	0.18
	O1	2.689(6)	0.14	O1	2.689(7)	0.14
	<Ca3-O>	**2.54**	**1.76**	<Ca3-O>	**2.54**	**1.74**
Ca4 (CN6)	3 *x* O1	2.531(6)	0.22	3 *x* O1	2.404(8)	0.31
	3 *x* O9	3.119(9)	0.04	3 *x* O9	2.75(1)	0.12
	<Ca4-O>	**2.82**	**0.78**	<Ca4-O>	**2.58**	**1.29**
Ca5 (CN6)	3 x O4	2.211(9)	0.52	3 x O4	2.12(1)	0.50
	3 x O7	2.312(9)	0.39	3 x O7	2.25(1)	0.35
	<Ca5-O>	**2.26**	**2.73**	<Ca5-O>	**2.18**	**2.55**

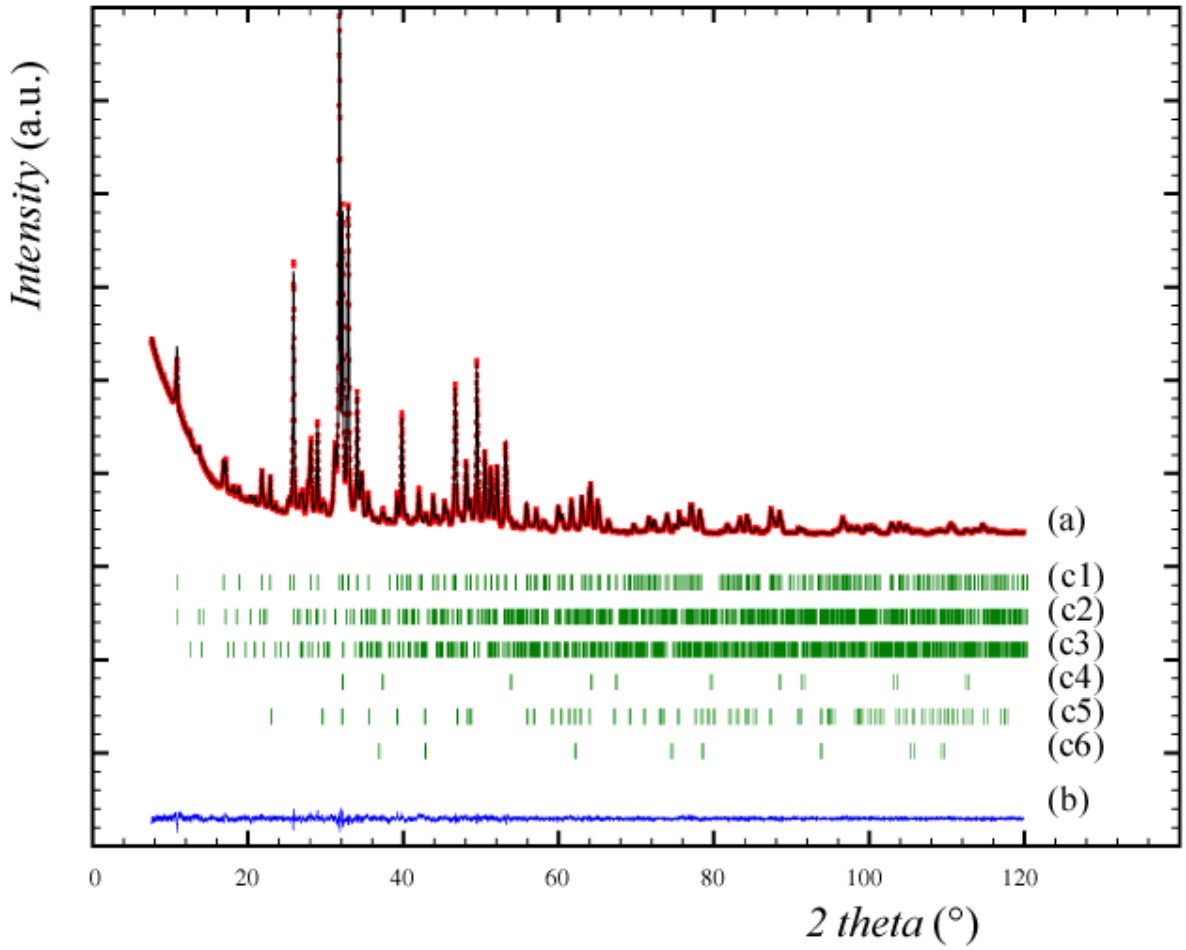

Figure SI1. Rietveld plot on the 5% Mg-doped sample calcined at 700°C, 50Mg700 sample, (λ = 1.5418 Å). Observed (a; dots), calculated (a; line) and difference (b line) powder diffraction patterns are presented. Bragg positions are indicated by vertical bars for hydroxyapatite (c1), whitlockite (c2), α-$Ca_2P_2O_7$ (c3), lime (c4), calcite (c5) and periclase (c6).

The horizontal difference curve (Figure SI1, curve b) gives evidence of the accuracy of the refinements performed for all the powder patterns.

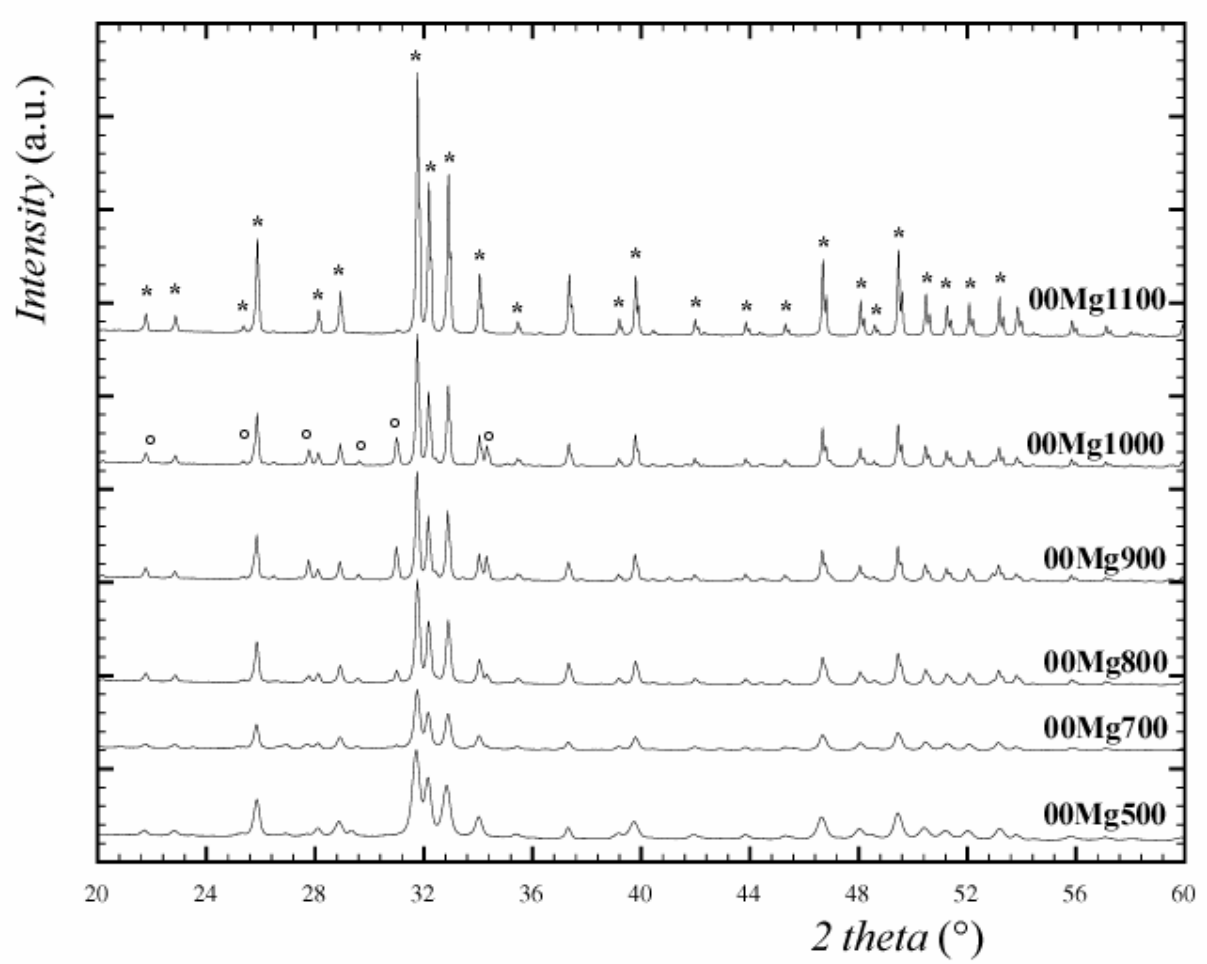

Figure SI2. Details of the X-rays powder patterns (in the range $20 < 2\theta < 60°$) from the Mg free BCP series with calcination temperature from 500°C to 1100°C. The marks ***** and ° indicate respectively the main diffraction peaks of hydroxyapatite (HAp) and β-TCP phases.

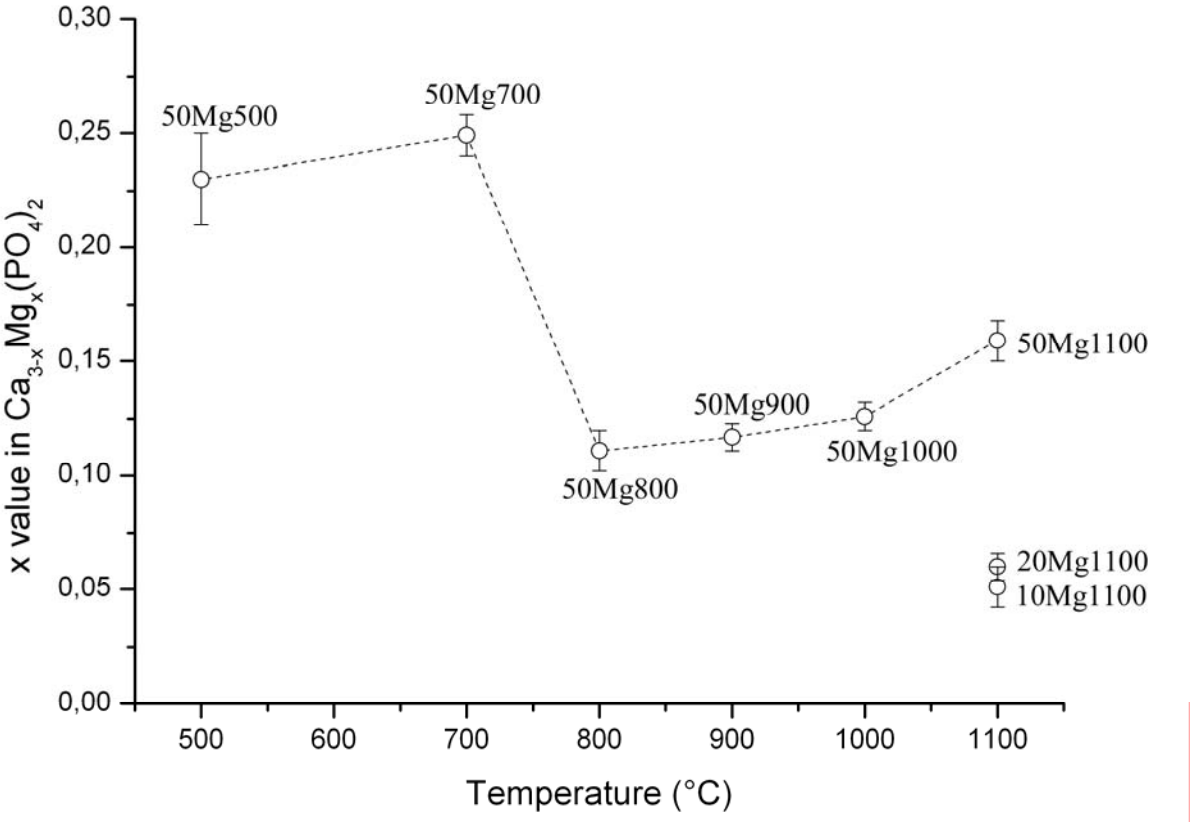

Figure SI3. Ca substitution level in the $Ca_{3-x}Mg_x(PO_4)_2$ solid solution for the 50Mg series and for the samples 20Mg1100 and 10Mg1100.

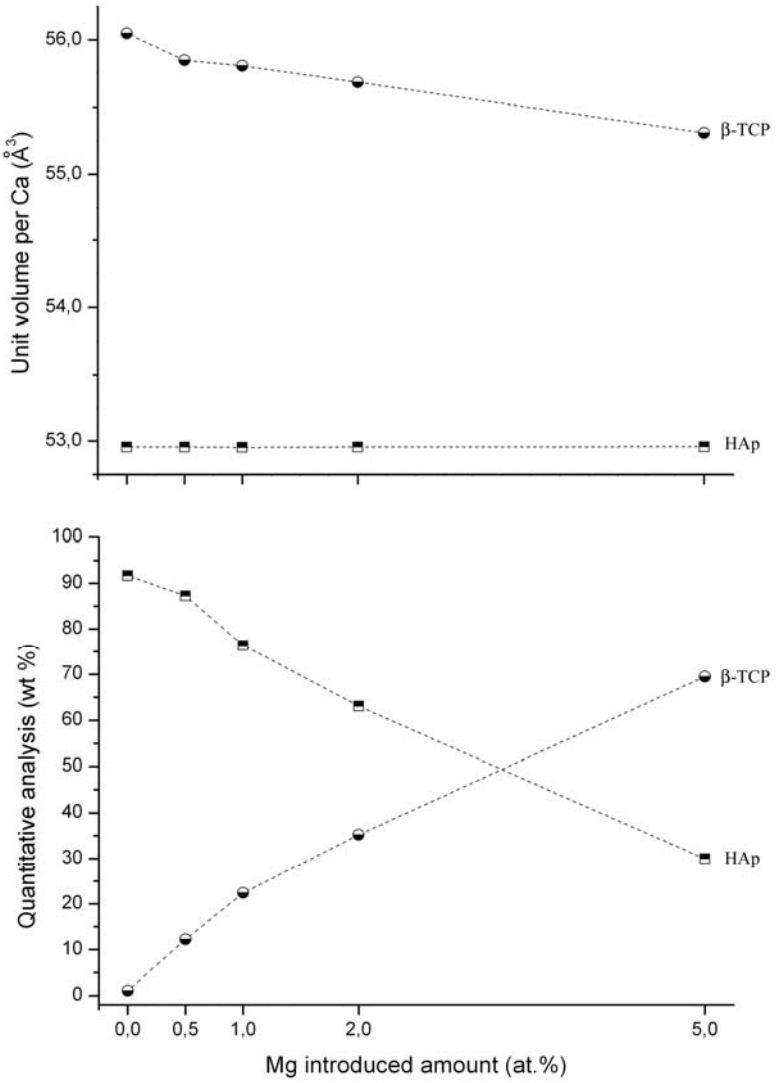

Figure SI4. Results of the Rietveld refinements as a function of the introduced Mg amount at 1100°C: (bottom) quantitative phase analysis, (top) unit volume per Ca = unit cell volume/unit cell number of Ca atoms. Results are represented for the HAp phase (squares) and the β-TCP phase (circles). Dashed lines are only guides for eyes.